Journal of Power Sources 195 (2010) 4570–4582

Contents lists available at ScienceDirect

Journal of Power Sources

journal homepage: www.elsevier.com/locate/jpowsour

Review

Progress in metal-supported solid oxide fuel cells: A review

Michael C. Tucker*

Materials Sciences Division, Lawrence Berkeley National Laboratory, 1 Cyclotron Rd, MS 62-203, Berkeley, CA 94720, United States

ARTICLE INFO

Article history:
Received 14 January 2010
Received in revised form 11 February 2010
Accepted 12 February 2010
Available online 20 February 2010

Keywords:
SOFC
Metal-supported
Fuel cell materials

ABSTRACT

Metal-supported solid oxide fuel cells provide significant advantages over conventional ceramic cells, including low materials cost, ruggedness, and tolerance to rapid thermal cycling and redox cycling. Various metal-supported cell designs have been developed, utilizing a range of electrolyte, electrode, and support materials prepared by various fabrication and deposition techniques. This paper reviews the current state of metal-supported cell technology and suggests opportunities for further development.

Contents

* Tel.: +1 510 486 5304; fax: +1 510 486 4881.
E-mail address: mctucker@lbl.gov.

0378-7753/$ – see front matter © 2010 Elsevier B.V. All rights reserved.
doi:10.1016/j.jpowsour.2010.02.035

1. Introduction

Solid oxide fuel cell (SOFCs) development has occurred worldwide for many decades. Continuous improvement in materials, cell design and manufacturing processing have resulted in a very high level of technical refinement. Successful commercialization of traditional SOFC technology, however, has been precluded by a number of factors including: high cost of cell materials; unreliable cell sealing; susceptibility of the cell to failure due to rapid thermal transients, mechanical shock, or oxidation of the anode; and, manufacturing issues associated with high-yield production of large, complex ceramic parts. Alternative metal-supported SOFC designs have attracted renewed interest in recent years, driven by their low materials cost, ruggedness and abuse tolerance, and manufacturability benefits. This paper provides an overview of the metal-supported SOFC field, including various cell design and manufacturing strategies, technical achievements to date, and recommendations for further development.

1.1. Conventional SOFC designs

The majority of SOFC development to date focuses on electrolyte-supported cells (ESCs), cathode-supported cells (CSCs), or anode-supported cells (ASCs). The ESC design utilizes a thick electrolyte layer to provide mechanical support for thin anode and cathode layers. Efficient cell operation is possible when the ohmic impedance of the electrolyte is minimized. This can be achieved by utilizing a relatively high operating temperature, as the conductivity of typical SOFC electrolytes displays Arrhenius-dependence on temperature [1]. Thus, ESCs with 100 μm–1 mm electrolyte, thick enough to provide mechanical support for the cell, are typically operated in the range 850–1000 °C. Such high cell temperatures require significant thermal insulation and expensive high-temperature materials to be used in the stack and balance-of-plant (BOP). Alternatively, the ohmic impedance of the electrolyte may be decreased simply by making it thinner. The thin-electrolyte-film CSC and ASC designs were developed in part to reduce the operating temperature, enabling the use of more economical stack and BOP materials. Anode-supported electrolyte films are typically <50 μm thick, allowing operation below 800 °C. Cathode-supported films are similarly thin, although operating temperatures are generally higher to overcome limitations in the coarse cathode structure.

In the ESC, CSC, and ASC cases, the mechanical support is a brittle ceramic or cermet, and contains expensive materials. In contrast, the metal-supported cell (MSC) design utilizes ceramic layers only as thick as necessary for electrochemical function (within processing constraints); the mechanical support is made from inexpensive and robust porous metal, and the electrochemically active layers are applied directly to the metal support, as shown in Fig. 1. As discussed in this paper, this MSC design provides significant cost, manufacturing, abuse tolerance, and operational advantages that make it a very promising candidate for commercialization.

Many SOFC applications would benefit greatly from increased mechanical ruggedness, redox tolerance, and rapid thermal cycling promised by metal-supported cells. The benefits of mechanical ruggedness are obvious for portable applications where the cell or stack is likely to experience shock, vibration, or mechanical loading. Ruggedness is also expected to improve manufacturability, as cells can withstand rough or fast handling operations that would fracture a ceramic cell. Flexibility of the cell also means that camber can be flattened out during stacking. Redox cycling tolerance is important because it allows cells to accept cooling without the need for blanketing, interruption in fuel supply, and catalyst oxidation at high current density. Ability to withstand these circumstances can reduce balance-of-plant complexity and redundancy. Rapid thermal cycling is of course also desirable for many SOFC applications

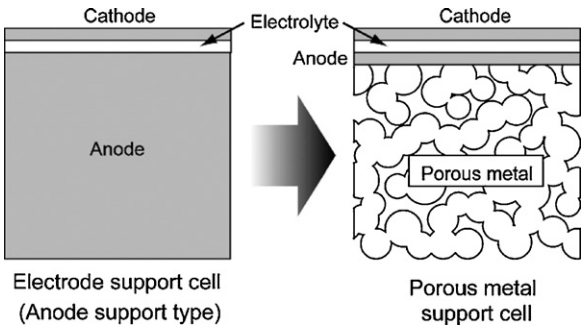

Fig. 1. Schematic representation of anode-supported cell (ASC) and metal-supported cell (MSC). Only a thin portion of the anode layer, as required for electrochemical function is retained in the MSC design. Reproduced with permission from Ref. [41].

Aside from application requirements, there is an additional reason to minimize heating and cooling times for metal-supported cells. At the operating temperature, initial thermal stresses in the cell due to CTE mismatch between the electrolyte and metal support are expected to dissipate via metal creep. After sufficient time at the operating temperature, a "zero-stress" state is achieved. The CTE of the metal support is typically somewhat higher than that of the electrolyte. Therefore, as the cell cools the electrolyte is held in compression, a desirable situation for mechanical integrity of the cell. If the cell is cooled and reheated quickly enough, the electrolyte will continue to be in compression until the operating temperature is reached again. In contrast, if the cell is cooled very slowly, creep can continue to relax stress in the cell, and a new "zero-stress" state will occur at a temperature that is lower than the operating temperature. Upon reheating, then, the electrolyte will initially be in tension at the operating temperature. Therefore, cooling and reheating quickly enough to maintain the operating temperature as the "zero-stress" state is desirable.

1.2. Early MSC development

The advantages of a metal-supported SOFC design were first recognized in the 1960s [2]. This early work used flame-spray deposition of zirconia-based electrolyte onto presintered austenitic stainless steel supports. Cells were operated in the range 700–800 °C, producing an impressive at that time 115 mW cm^{-2} at 750 °C. Cell operation with hydrogen, methanol, and kerosene as fuels was demonstrated. In the 1990s, prefabricated tubular NiCrAlY [3] and planar $CrFe_5Y_2O_3$ [4] supports were coated with plasma-sprayed zirconia electrolytes. Power densities approaching 1 W cm^{-2} were achieved at 900 °C. Near the turn of the century, colloidal and wet-chemistry methods for applying and sintering thin films of electrolyte onto anode supports were recognized as suitable for metal-supported cell designs as well. These inexpensive deposition techniques resulted in thinner electrolytes that could be operated at lower temperatures compatible with low-cost ferritic stainless steels. This approach was pioneered at Imperial College/Ceres Power for CGO electrolyte [5,6], and at LBNL for YSZ electrolyte [7].

2. Choice of metal for support

Metal-supported solid oxide fuel cells have recently been prepared on supports with a variety of metal compositions, including Ni, FeNi, NiCrAlY, and ferritic stainless steel. Table 1 lists some relevant features of several candidate materials. It is desirable to match the coefficient of thermal expansion (CTE) of the metal to that of

Table 1
Summary of candidate support metals.

Metal	CTE (ppm K^{-1})	Cost ($/kg 2009)	Relative oxidation resistance
NiCrAlY	15–16	63	Excellent
Hastelloy-X	15.5–16	22	Excellent
Ni	16.5	18	None[a]
Ni–Fe (1:1)	13.7	9	None[a]
300-Series stainless steel	18–20	2	Poor
400-Series stainless steel	10–12	2	Very good

Note that CTE of electrolytes (YSZ, CGO, LSGM) are 10–12 ppm K^{-1}.
[a] Readily oxidizes in air or during cooling in fuel Refs. [20,22,68–70].

the electrolyte to enable rapid thermal cycling. Low-cost and low-oxidation rate are also preferred. Although most metal-supported SOFC developers use planar supports, tubular supports are gaining popularity [8–12].

2.1. Ni-based materials

Early work used thick plasma-sprayed yttria-stabilized zirconia (YSZ) electrolyte applied to porous NiCrAlY metal supports prepared by die pressing [3]. The excellent oxidation resistance of the NiCrAlY alloy allowed operation up to 900 °C, so reasonable performance was obtained despite the thick electrolyte.

Recently, several groups have used porous pure Ni as a support material. The high cost of Ni, poor CTE match to the electrolyte, low redox tolerance, and susceptibility to coking and sulfur damage present strong limitations to the utility of this support material. Micro-fuel cells were fabricated on porous pure Ni tubes [13]. Using the oxidation/reduction technique, 1-mm diameter Ni tubes were prepared with pores in the 0.5–2.5 μm range. YSZ was then deposited directly onto the Ni by EVD. Thus, the Ni tube functioned as both support and anode. The CTE of Ni is substantially higher than that of YSZ (see Table 1). In this case, however, thermal stress was mitigated in this design by a relatively low YSZ deposition temperature of 1000 °C and very small tube diameter. Porous Ni has also been used as the support for Ni-YSZ/LSGM/LSCF layers deposited by atmospheric plasma spray (APS) deposition [14]. After spraying, the layers were sintered at 1000 °C: low enough to avoid significant reaction between LSGM and Ni, and high enough to provide gas-tight layers and reasonable power density of 440 mW cm^{-2} at 800 °C. Functional cells have also been produced by co-sintering a Ni support/Ni-YSZ anode/YSZ electrolyte trilayer structure at 1400 °C in reducing atmosphere [15]. Although significant coarsening of the anode Ni occurred during sintering, reasonable power density of 470 mW cm^{-2} was achieved at 800 °C.

Ni–Fe supported SOFCs with LSGM/SDC [16–19] and GDC [20,21] electrolyte have also been prepared. The addition of Fe mitigates the cost and CTE mismatch of pure Ni, but susceptibility to sulfur, coking, and redox intolerance remain. Ni–Fe alloy is strong and relatively straightforward to produce. Supports are typically prepared as mixtures of Fe_2O_3 and NiO and sintered to near full density. This facilitates application of a thin, continuous electrolyte layer as the green electrolyte does not need to bridge pores in the support. The support is reduced to Ni–Fe alloy in the SOFC fuel stream upon cell start-up. The volume contraction associated with this reduction opens sufficient porosity in the support to enable adequate fuel transport. In this design, the Ni–Fe support may also function as the anode. A study of anodic overpotential comparing pure Ni and a range of Ni alloys containing 10 wt% alloying element found that Ni–Fe exhibited the best performance [16]. Ishihara et al. have continued to use roughly 10 wt% Fe as the preferred composition [16–19]. The addition of more Fe to Ni improves the CTE match to the electrolyte and reduces the material cost. Alloys with a range of Fe–Ni compositions were studied, and those with close to 1:1 weight ratio were found to have the CTE best match to YSZ [22]. Micro-fuel cells with <20 μm thin films of Ni–Fe (1:1, w/w) and <2 μm GDC electrolyte have been fabricated [20]. A variety of other Ni–Fe compositions has been used with Ni-GDC anode layer and GDC electrolyte [21]. A starting material of NiO–Fe_2O_3 (70–30 mol%) was selected, as higher iron contents led to delamination during cell testing.

2.2. Iron-based materials

Most developers favor ferritic stainless steel for the metal support. Ferritic stainless steels are body-centered cubic, ferromagnetic alloys containing primarily iron and chromium with very low carbon content. Typical alloy designations include 430, 409, 410, and 441. These alloys are widely used for automotive exhaust manifolds and mufflers because of their low-cost and high-temperature oxidation resistance. Ferritic stainless steel typically contains at least 10.5 wt% Cr to form a continuous chromia scale, and no more than 26 wt% Cr to avoid formation of the brittle sigma phase at higher Cr content. The alloys often include Ni, Mo, Si, Ti, Al and others to improve various physical properties. There are a number of advantageous properties of ferritic stainless steels that recommend them for application as the mechanical support for SOFC devices. They are quite inexpensive (Table 1), produce a thin, continuous, conductive chromia scale, and can have very long lifetimes at the SOFC operating temperature as discussed below. Furthermore, their CTE is around 10–12 ppm $°C^{-1}$ and therefore compatible with YSZ and CGO. It is widely known that addition of Al can improve oxidation resistance by forming an Al_2O_3 scale at the surface of the steel, and addition of Si can improve chromia scale adhesion by forming SiO_2 subscale between the scale and bulk. The relatively high conductivity of the protective chromia oxide scale [23] is of critical importance, however, for maintaining acceptable contact resistance at the support/electrode interface. Therefore, addition of Al or Si must unfortunately be avoided, as the scales they form are non-conductive. Likewise, 300-series stainless steels rapidly form non-conductive mixed Fe–Cr-oxide scales at SOFC operating temperatures [24], and have a much higher CTE. Some of these issues are explored in more depth in the context of metallic interconnects for SOFCs in a review by Yang [25]. For the above reasons, ferritic stainless steel is the alloy of choice for metal-supported SOFCs.

Ferritic stainless steel supports have been prepared by laser drilling to form a perforated sheet [5,6,26] and standard powder-metallurgy methods, including tape-casting [27], and isostatic pressing [7–9,12]. Highly porous stainless steel parts are also routinely fabricated by extrusion and free-powder sintering [28], and these methods are expected to have benefits for high-volume manufacturing. Laser drilling a preformed sheet provides a smooth, well-defined surface on which to deposit the electrochemically active layers. Introduction of a high enough density of 10–30 μm holes was found by gas diffusion modeling to be enough to support adequate diffusion of reactant through the support into the active layers [29]. This has been confirmed experimentally [5,6,26]. Of course, a prefabricated sheet will not shrink during further processing of the electrochemical layers. This is acceptable for CGO, which

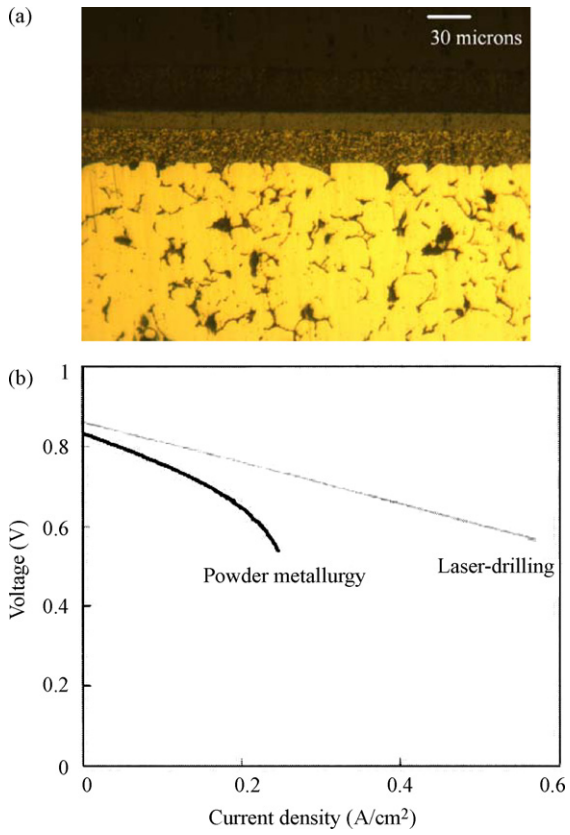

Fig. 2. (a) Cross-section image of metal-supported cell with support prepared by powder metallurgy. The relatively dense support gives rise to the mass transport limitation observed in (b) during testing at 600 °C with hydrogen and air. Reproduced with permission from Ref. [26].

can be constrained-sintered to full density, or for plasma spray deposition of YSZ, but precludes co-sintering of YSZ electrolyte. The same holds true for powder-metallurgy supports. Presintered supports that do not shrink during cell processing have been used with CGO [26,30–35] and thermally sprayed YSZ [36–40], whereas co-sintering of support and electrolyte layers must be used for wet or colloidal YSZ deposition processes [7–9,11,12]. Whether a powder-metallurgy support is presintered or co-sintered with the electrolyte in place, it must maintain sufficient porosity after cell preparation to provide adequate gas transport. Appropriate steps to achieve the desired final porosity must be taken, or else the dense support structure can impose a severe limiting current density due to concentration polarization, as seen in Fig. 2. Final support porosity depends on sintering temperature, particle size, particle size distribution, alloy composition, particle morphology, poreformer, binder, and shrinkage of the other layers. Some guidance for navigating these complex interrelationships is provided by Kurokawa et al. [41] In that work, 410 l stainless steel powder was mixed with aqueous acrylic binder and PEG poreformer. Water-atomized powder was chosen because it has a much rougher morphology than gas-atomized powder. This results in lower packing density and therefore higher initial porosity. Mechanical interlocking between the rough particles also improves handling strength in the green and debinded states. Detailed maps of final density and shrinkage as a function of metal particle size and poreformer/binder content were presented. Smaller metal particles led to higher shrinkage, which is good for matching to YSZ shrinkage, but also to lower final porosity. Porosity can be improved by increasing the binder and poreformer content, but at the expense of total shrinkage. Clearly, some optimum binder/poreformer content must be determined for a given metal powder.

In summary, a variety of metal support compositions and structures have been incorporated into functioning SOFC devices. Ferritic stainless steels are the preferred material, because of their low-cost, CTE match to common electrolyte materials, formation of conductive protective scales, and adequately low oxidation rate.

2.2.1. Suitable operation temperature window

The selection of ferritic stainless steel as the preferred metal support imposes a relatively narrow acceptable operation temperature window. The desire for high electrochemical performance and rapid internal reforming of hydrocarbons prescribes a high operating temperature (generally accepted as above 625–650 °C), which is balanced by the need for long stainless steel lifetime. A brief discussion of stainless steel oxidation is provided below. Reviews of stainless steel behavior in SOFC environments have been published, e.g. [42,43] and the reader is referred to these for more detail.

The formation of a continuous, protective Cr_2O_3 scale on ferritic stainless steel is critical for longevity of a metal-supported SOFC. In many other applications, stainless steel is used as a mechanical component. In that case, integrity of the protective scale is not as critical a concern. Spallation (cracking and delamination of the oxide scale) exposes fresh surface which then oxidizes to renew the protective scale. As an SOFC support, however, the stainless steel is also an electrical component, collecting current from the electrodes. Current passes between the electrode and the metal support through the chromia scale. In this case, spallation would lead to electrical disconnection of the electrochemically active area and therefore cannot be tolerated. Counterintuitively, the oxygen partial pressure is sufficiently high in both the anode and cathode chambers that Cr_2O_3 scale growth kinetics are controlled by solid-state diffusion through the oxide scale and the observed oxidation rate is roughly the same for stainless steel contacting air or fuel [42,44]. It has also been found that the presence of moisture does not affect oxidation rate significantly [45]. It should be noted, however, that Cr evaporates from the scale in air and the presence of moisture greatly accelerates the evaporation rate. This is discussed further in Section 4.

Although chromia is highly electronically conductive compared to other protective scales such as silica or alumina, it is the least conductive material in the electrical path from power leads to the electrode/electrolyte interface. In addition to increasing the risk of spallation discussed below, formation of thick chromia scales is expected to introduce significant increase in cell resistance. Using the conductivity of bulk Cr_2O_3 at 700 °C provided in Ref [46], roughly 10 mOhm cm^{-2} increase in ASR is expected for each micrometer of scale growth. Predicting the electrical impact of *in situ* protective scales, however, is quite complicated. The apparent conductivity of protective scales may differ substantially from the bulk Cr_2O_3 value due to differences in dopant and defect concentration or the presence of minor phases or microvoids in the scale. Limited data exists comparing bulk Cr_2O_3 and *in situ* scale conductivities. Conductivity of scales grown on various chromia-forming alloys has been reported to differ from the bulk value by up to two orders of magnitude [47,48]. Furthermore, most literature pertains to properties of scales formed in air or oxidizing atmosphere. Hou and Stringer [23] found that stainless steel scales formed in anode conditions (850 °C, moist hydrogen) displayed several times higher resistance than those formed in air. A similar trend was reported by Holt and Kofstad [46], and reproduced in Fig. 3. They found that the conductivity of porous bulk Cr_2O_3 is reduced in the presence of hydrogen, and suggested that hydrogen dissolution into Cr_2O_3 affects the defect structure. The effect is exacerbated significantly at temperatures below 600 °C. This is of particular concern for CGO-based metal-supported SOFCs operating in the 500–600 °C range. There is a clear need for measurement of the electrical conductivity of real scales formed on relevant stainless steel com-

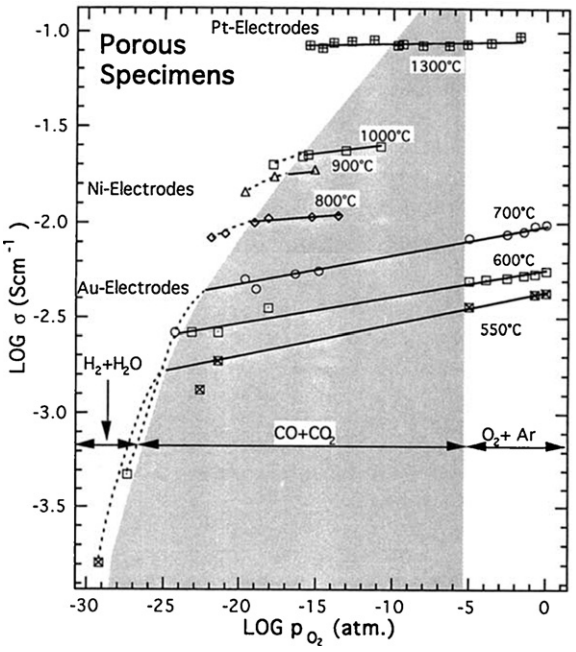

Fig. 3. The electrical conductivity of two porous chromia specimens (B/1300 °C and D/all other temperatures) as a function of the partial pressure of oxygen at temperature from 1300 to 550 °C. Different electrode materials were used: Pt at 1300 °C, Ni at 800–1000 °C and Au < 700 °C. The ambient oxygen pressures were established with O_2 + Ar, CO + CO_2 and H_2 + H_2O. Reproduced with permission from Ref. [46].

positions in temperature ranges and atmospheres relevant to SOFC operation.

The upper acceptable operating temperature is determined by oxide growth kinetics and desired SOFC device lifetime. Failure of the device will occur when the Cr_2O_3 scale becomes thick enough that spallation occurs. Thus, expected lifetime is a strong function of temperature. Fig. 4 shows scale thickness vs. time for various parabolic oxidation growth rate constants calculated according to the parabolic growth rate law:

$$L^2 = \frac{k_p t}{\rho\theta} \quad (1)$$

where L is the scale thickness (cm), k_p is the parabolic growth rate constant referring to oxygen mass uptake ($g^2\ cm^{-4}\ s^{-1}$), t is time (s), ρ is the density of the scale ($g\ cm^{-3}$), and θ is the weight fraction of oxygen in the scale. Setting a maximum acceptable scale thickness to avoid spallation allows us to determine expected lifetime for a given growth rate, or conversely, to set maximum allowable growth rate for a desired lifetime. The addition of reactive elements (Y, La, Ce, etc.) to the stainless steel is well-known to improve scale adhesion and reduce oxidation rate [23,43]. The results reported in

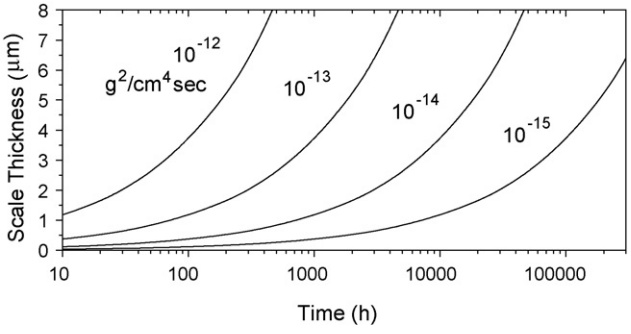

Fig. 4. Chromia scale thickness as a function of oxidation time calculated by Eq. (1) for various oxidation growth rate constants.

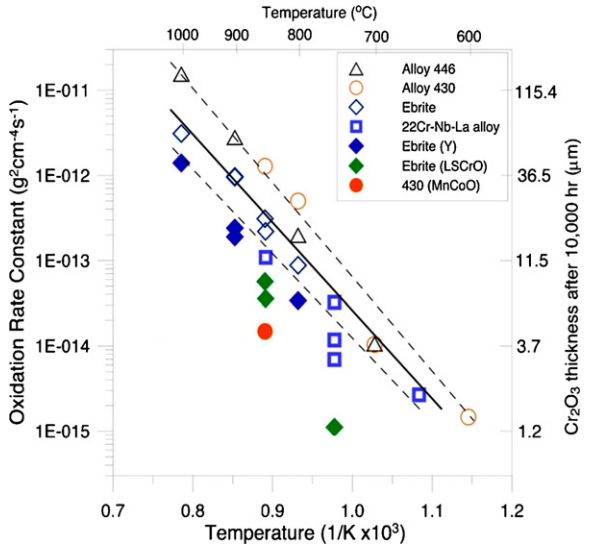

Fig. 5. Oxidation rate constant as a function of temperature for various ferritic stainless steels. Closed symbols refer to steels coated with the material listed in the legend. Reproduced with permission from Ref. [50]. Lines provide a guide to the eye to define the range of oxidation rates for uncoated steels.

Ref. [49] suggest that with an yttria-treated steel operating below 800 °C, adherent scales 3 μm thick and possibly thicker can be expected before failure is likely. Referring to Fig. 4, a 3 μm acceptable scale thickness implies maximum oxidation rates of slightly above $10^{-14}\ g^2\ cm^{-4}\ s^{-1}$ for desired lifetimes of greater than 5000 h and slightly above $10^{-15}\ g^2\ cm^{-4}\ s^{-1}$ for desired lifetimes of greater than 50,000 h. In the temperature range 600–950 °C, ferritic stainless steels form the desired continuous, protective Cr_2O_3 scale. Fig. 5 shows measured oxidation rate constants for a variety of ferritic stainless steels as a function of temperature [50]. To achieve the oxidation rates required for 5000 h lifetime the maximum temperature is about 800 °C, whereas for lifetimes greater than 50,000 h (as required for stationary power plants) the maximum acceptable temperature is in the 650–700 °C range. This lower temperature makes achieving high power a challenging proposition. Note that, as discussed below, most groups demonstrating metal-supported cells with YSZ electrolyte report performance and testing at 800 °C. Operating at such a high-temperature limits the expected lifetime to several thousand hours. There is ample evidence that appropriate coatings, treatments, or alloy modifications can reduce the oxidation rate and improve scale adhesion for dense interconnect materials, thereby improving expected lifetime before failure via scale spallation. Exploring the effects of similar treatments on oxidation of porous stainless steel supports seems to be a fruitful area for further work.

3. Choice of electrolyte

3.1. LSGM

Strontium- and magnesium-doped lanthanum gallate (LSGM) has been successfully applied as an electrolyte on Ni metal supports using atmospheric plasma spray (APS) [14] and on Ni–Fe metal supports using pulsed laser deposition (PLD) [16–19]. The prime advantage of this material is that it is a nearly pure ionic conductor and exhibits good oxygen ion conductivity at temperatures as low as 400 °C. However, this electrolyte is fairly reactive, making long-term stability a concern. LSGM has been shown to react with Cr_2O_3 and Cr-containing vapors [51], limiting use with stainless steel supports. LSGM also reacts with Ni in the anode or Ni–Fe metal support. Application of an additional thin SDC layer

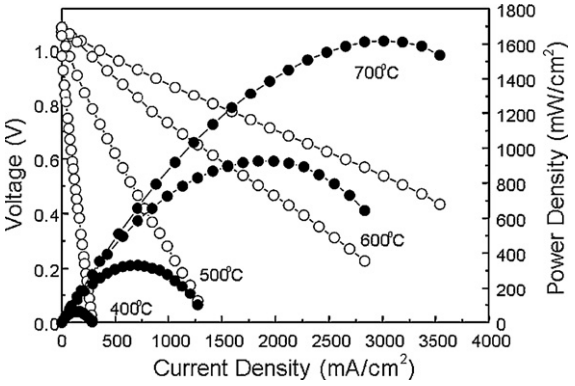

Fig. 6. Performance of a cell prepared with NiFe support, LSGM/SDC bilayer electrolyte and SSC cathode. Cell was operated with moist hydrogen and oxygen. Reproduced with permission from Ref. [17].

deposited by PLD between the electrolyte and metal support is sufficient to prevent reaction [17,19]. Cells with this design provide impressive power densities ranging from 100 mW cm^{-2} at 400 °C to 1.6 W cm^{-2} at 700 °C, as shown in Fig. 6. These values were obtained after a moderately fast initial heat up (50 °C min^{-1}). The reported power density dropped by roughly 50% upon cooling and heating a second time. It is not clear whether this was due to thermal cycling or reoxidation of the support during cooling. Long-term operation has not been reported.

3.2. CGO

SOFCs with gadolinium-doped ceria (CGO) electrolyte have been prepared on Ni–Fe [21], Hastelloy-X [32,33,35], and ferritic stainless steel [5,6,26,29–31,34] supports. The first key advantage of ceria-based electrolytes is that they display high conductivity and can therefore be used at lower temperatures relative to YSZ. Acceptable conductivity of the CGO electrolyte can be achieved above about 500 °C, setting the lower operating temperature limit [5]. A key challenge arises, however, because Ce^{4+} ions in CGO can be reduced to Ce^{3+} in the fuel atmosphere, with significant reduction above about 600 °C. This creates lattice expansion stress, and the electrolyte becomes a mixed conductor, reducing the efficiency and performance of the device. As seen in Figs. 7 and 8, open circuit voltage (OCV) can drop to below 0.8–0.9 V at 600 °C and higher due to mixed conduction in the electrolyte, setting this as the maximum operating temperature [5,35]. It should be noted that mixed conduction is predicted to be minimized at high current density, as the partial pressure of oxygen at the electrolyte/anode interface increases [29]. The low operating temperature of 500–600 °C imposes a critical system limitation, in that pre-reforming of hydrocarbon fuels is generally required [5,6] adding expense and complexity to the system.

The second key advantage of ceria-based electrolytes is the possibility of constrained-sintering to full density, allowing the use of a prefabricated support that shrinks very little or not at all during electrolyte processing. The addition of sintering aids to CGO to improve low-temperature sintering is well-known [e.g. 52–54]. Ceres Power reported electrophoretic deposition of CGO onto anode material supported by laser-perforated stainless steel sheet, followed by sintering to full density below 1000 °C [5]. At such low temperatures, it is possible to sinter CGO on a stainless steel substrate in air, a simpler alternative to typical higher temperature sintering which must be performed in reducing atmosphere to protect the substrate from excessive oxidation. More recently, wet colloidal deposition of CGO with Fe sintering aid followed by sintering at 1050 °C was reported [26].

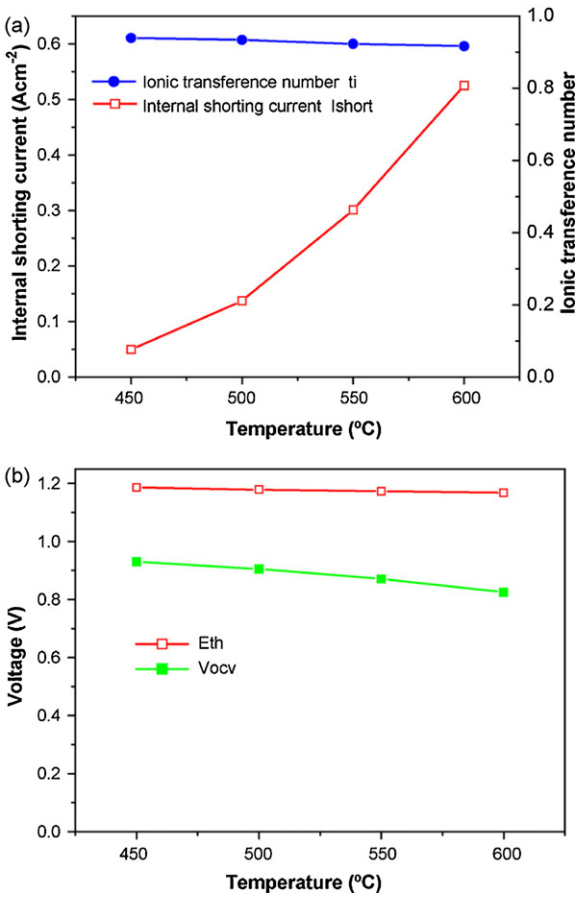

Fig. 7. Internal short-circuiting due to mixed conductivity of ceria-based electrolyte for a metal-supported cell with Ni-SDC anode, SDC electrolyte, and SSC-SDC cathode operated with humidified hydrogen and air. Analysis of (a) ionic transference number *ti* and internal shorting current *I*short and (b) theoretical open circuit voltage *E*th and measured open circuit voltage *V*ocv over 450–600 °C. Reproduced with permission from Ref. [35].

Other processing routes for preparing CGO electrolyte layers on metal supports have included: drop-coating followed by sintering at 1450 °C in air [21], and RF magnetron sputtering [20] using Ni–Fe oxide support; pulsed laser deposition onto 430 stainless steel and Hastelloy-X [30,32]; spray pyrolysis onto 430 stainless steel [31]; and, various plasma spray techniques onto Hastelloy-X [33–35].

Recognizing the mixed conduction of ceria as a limitation to overall system performance, Hui et al. [30,32] added a thin layer of Sc-stabilized zirconia (ScSZ) between the anode and CGO electrolyte to block electronic conduction. Because PLD was used to deposit both ScSZ and CGO, followed by sintering at a relatively low 850 °C, reaction was avoided and the intended phases were produced. The added complexity of the cell design is justified in that the additional ScSZ layer was effective at blocking electronic conduction through the bi-electrolyte layer. Fig. 8 shows the performance of a cell containing ScSZ/CGO bi-electrolyte; note the OCV values near 1.0, even for 600 °C. A similar approach was followed by Park and Virkar [21]; however, in this case the CGO/YSZ multi-layer electrolyte was prepared by wet deposition and fired at a relatively high temperature of 1450 °C. This led to reaction between the YSZ and CGO, thereby degrading the effectiveness of the YSZ layer. Only a very small increase in OCV was obtained, compared to a similar cell with no YSZ layer. These contrasting results highlight the key role of processing considerations when designing an effective cell structure.

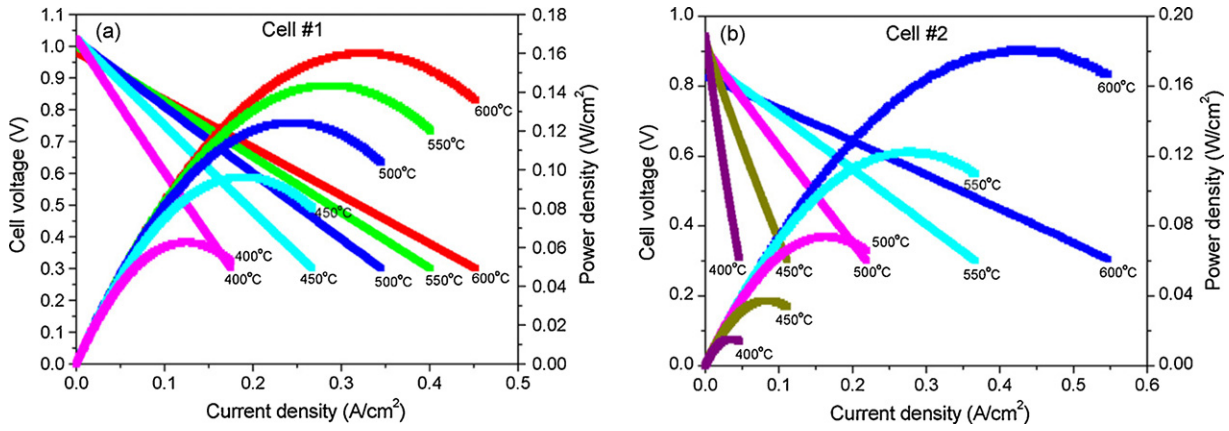

Fig. 8. Performance of metal-supported cells with Ni-SDC anode, SDC electrolyte, and SSC-SDC cathode operated with humidified hydrogen and air. Cell #1 (a) had an additional thin Scandia-stabilized zirconia (ScSZ) layer between the anode and SDC electrolyte to block electronic conduction. Reproduced with permission from Ref. [32].

3.2.1. Notable demonstrations with metal-supported cells using CGO electrolyte

Ceres Power has reported a number of encouraging operational modes [6], including: >2500 h continuous operation with hydrogen fuel; two fuel-starvation redox cycles and six thermal cycles (relatively slow at 8 h/cycle) with no loss of performance; and, operation on reformate fuel with minimal power loss compared to pure hydrogen. Ceres Power has not provided a public update of recent progress due to commercialization activities, however it is assumed that the current state of the art has surpassed the achievements listed above.

The best peak power density at 600 °C reported to date is about 0.5 W cm^{-2}, achieved with Hastelloy-X support and plasma thermal spray deposition of the CGO electrolyte [34]. Ten relatively fast thermal cycles (60 °C min^{-1}) were demonstrated [33,34] with significant degradation during the first two cycles and moderate degradation thereafter. The degradation was attributed to cathode cracking or delamination due to the large CTE difference between the electrolyte (12.7 ppm K^{-1}) and SSC/SDC cathode (18.4 ppm K^{-1}). Although this cathode issue must be addressed, it is encouraging to find that such rapid thermal cycling did not degrade the support/anode/electrolyte structure.

3.3. YSZ

YSZ offers several key advantages over the other electrolyte materials, and therefore many metal-supported SOFC developers choose to use YSZ electrolyte. The performance and longevity of YSZ are adequately demonstrated, and the cost is well-defined by the large amount of zirconia used in oxygen sensors. YSZ is a pure ionic conductor, allowing efficient operation at temperatures where CGO displays significant electronic conductivity. This provides the opportunity to operate in a temperature range where internal reforming can occur, i.e. above 650 °C, a significant benefit from a systems perspective. The main disadvantage of YSZ is that it cannot generally be sintered to full density in a constrained geometry. To date, developers of metal-supported YSZ SOFCs have faced a fundamental decision between two processing routes to overcome this limitation: deposition techniques such as plasma- or flame-spray that apply dense YSZ, or colloidal/wet deposition of YSZ powder onto a green substrate followed by co-sintering to full density. This section discusses these options in more detail.

3.3.1. Plasma-deposited YSZ electrolyte

An extensive review of the application of plasma techniques to production of various SOFC components was provided by Henne [55]. For metal-supported SOFCs, the key advantage of plasma deposition techniques is the ability to deposit a near-dense coating on a preformed substrate, perhaps followed by a relatively low-temperature thermal treatment for full densification. Avoiding high-temperature processing of the metal substrate can, in principle, allow high substrate porosity to be retained during fabrication of the electrochemical layers. Relatively thick electrolyte layers (30–70 μm) are deposited to ensure gas-tightness, however. Furthermore, the apparent ionic conductivity of plasma-sprayed electrolyte is significantly lower than for sintered YSZ [38]. These factors generally mean operating temperatures of at least 800 °C are required for acceptable electrolyte ohmic resistance. As discussed above in Section 2.2.1, this high operation temperature can lead to premature cell failure due to rapid oxidation of the support.

The majority of work in this area has been undertaken by the German Aerospace Center (DLR) and collaborators [4,36–38,55]. As early as 2000, complete cells with porous ferritic stainless steel support, Ni/YSZ anode, YSZ or ScSZ electrolyte, and LSM/YSZ layers were prepared by plasma spray of all the electrochemically active layers [4]. Careful variations in the spray parameters allowed dense electrolyte and porous electrodes to be obtained, although increasing the porosity of the cathode in particular was seen as an area requiring improvement. Sufficient anode porosity is easier to obtain, as NiO is typically deposited and reduction to Ni during SOFC operation is accompanied by an increase in porosity. Further improvement in spray parameters (such as chamber pressure, plasma enthalpy, and plasma gas composition) has led to production of electrode layers with increased porosity, and greater than 750 mW cm^{-2} peak power has been achieved at 800 °C [38]. The resulting structure is shown in Fig. 9. Another strategy is to use conventional wet-processing techniques (which can easily include pore-forming means) to deposit the electrodes, and reserve plasma spraying for the electrolyte only [39]. Initial power density above 500 mW cm^{-2} was achieved at 800 °C.

3.3.2. Co-sintered YSZ electrolyte

In contrast to plasma techniques that apply a nearly dense electrolyte layer, there are many low-cost, high-throughput conventional ceramics processing methods that deposit a thin, porous layer of electrolyte particles. These can be classified as “wet” or “colloidal” deposition techniques, and include dip-coating, screen-printing, tape-casting, aerosol spray-coating, spin-coating, and drip-coating. Deposition occurs at low temperature, and produces a porous green layer generally consisting of particulates mixed with binder, poreformer (if porosity is desired), plasticizer, etc. In the case of YSZ electrolyte, deposition must be followed by binder burnout and a high-temperature sintering step to achieve full density of the layer (typically 1200–1400 °C). During sintering, the elec-

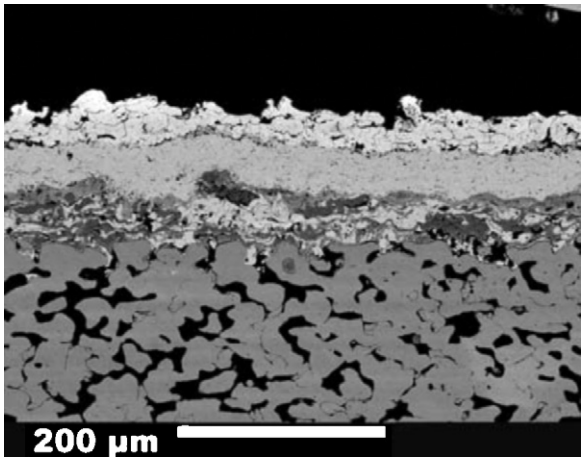

Fig. 9. Micrograph of cross-section of metal-supported cell with electrochemically active layers produced by plasma spray processing. Reproduced with permission from Ref. [38].

trolyte typically shrinks as much as 10–25%, depending on the green density achieved after deposition. Shrinkage of the metal support must be well-matched to that of the electrolyte; otherwise, the electrolyte layer is held in tension during co-sintering, resulting in cracks or insufficient densification. Specifying a metal support with good shrinkage-matching, while retaining sufficient porosity after sintering is challenging; sintering properties depend on metal composition, particle size, surface roughness, initial packing density, amount of poreformer and binder, and processing atmosphere [44].

Although achieving effective co-sintering of metal-supported YSZ electrolyte layers is challenging, many industrial development groups see these low-cost, high-throughput electrolyte deposition techniques as the key to cost-effective manufacture of metal-supported SOFCs. In addition to potential manufacturing advantages, the "wet" deposition processes allow relatively thin gas-tight electrolytes to be produced. YSZ electrolyte thickness in the range 10–20 μm is typical, allowing sufficiently low electrolyte ohmic resistance in the temperature range 650–700 °C. As discussed above, this relatively low operating temperature is necessary for long-term oxidation resistance of typical ferritic stainless steels. Originally proposed and developed by LBNL [7], co-sintering is pursued by Riso/Topsoe [27], Plansee [37], Ikerlan [10,11], JPower [12], and Worldwide Energy.

3.3.3. *Notable demonstrations with metal-supported cells using YSZ electrolyte*

Metal-supported cells with YSZ electrolyte have been operated for >2000 h continuously, with very promising abuse tolerance demonstrated.

Cells with plasma-sprayed YSZ electrolyte were operated with air and simulated reformate anode gas for over 2000 h at 800 °C with only 1% kh^{-1} degradation rate [38]. Similar cells experienced 20 redox cycles with no loss of OCV and less than 2.5% change in power density. These results are shown in Fig. 10.

Cells with co-sintered YSZ electrolyte and metal support have achieved greater than 1 W cm^{-2} at 700 °C as shown in Figs. 11 and 12 [8,27] and good stability has been observed over 1000 h testing [10,27]. Fig. 12 shows long-term operation of a cell with infiltrated ceria-based anode catalyst at about 650 °C. The degradation rate was less than 5% kh^{-1}. Excellent thermal cycling has also been demonstrated. LBNL has subjected braze-sealed tubular cells to extremely rapid thermal cycling (350–500 °C min^{-1}), and reports no OCV loss and minimal performance loss after 30 and 5 cycles, respectively [9,56]. Survival of several deep redox

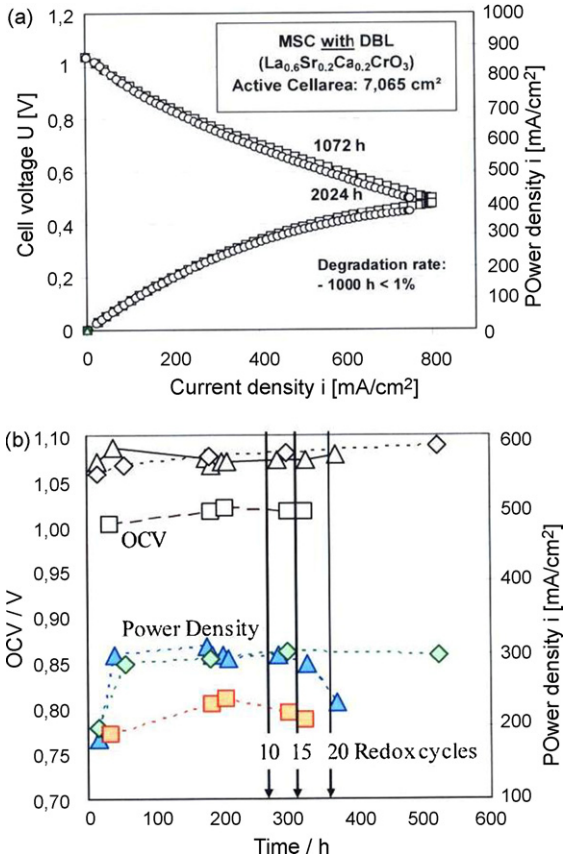

Fig. 10. (a) Performance of metal-supported cell with diffusion barrier layer (DBL), Ni-YSZ anode, YSZ electrolyte, and LSM cathode prepared by plasma spray processing at roughly 1000 and 2000 h operation. (b) Open circuit potential (OCP) and power density recorded at various times during operation with occasional redox cycles. Squares, triangles, and diamonds refer to cell development generations 1, 2, and 3, respectively. Operation was with simulated reformate and air at 800 °C. Reproduced with permission from Ref. [38].

cycles completed by switching between air and fuel at the operating temperature was also reported [9]. Ikerlan has demonstrated minimal performance loss after 250 thermal cycles from 80 to 800 °C at 10 °C min^{-1} heating and cooling rates, as shown in Fig. 13 [10]. It is expected that mechanical abuse tolerance will also be greatly improved relative to conventional ceramic SOFCs, but this is yet to be demonstrated quantitatively.

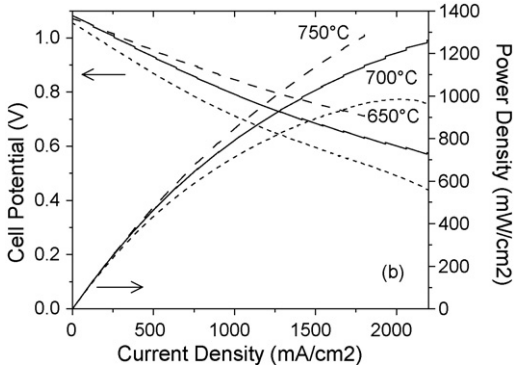

Fig. 11. Performance of co-sintered metal-supported cell with YSZ electrolyte, porous stainless steel support and current collector (as shown in Fig. 15). Ni anode catalyst and LSM cathode catalyst were introduced into porous YSZ electrode layers by infiltration. Operation was with humidified hydrogen and oxygen. Reproduced with permission from Ref. [8].

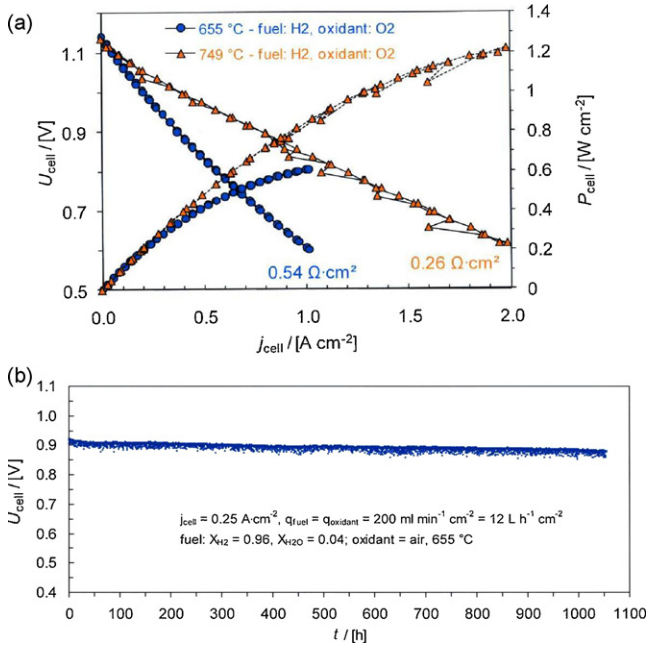

Fig. 12. (a) Initial performance and (b) long-tem operation of a metal-supported cell with co-sintered support/anode/electrolyte and LSCF/CGO cathode. Porous YSZ/stainless steel anode layer was infiltrated with CGO/Ni mixture. Operation with humidified hydrogen and (a) oxygen or (b) air. Reproduced with permission from Ref. [27].

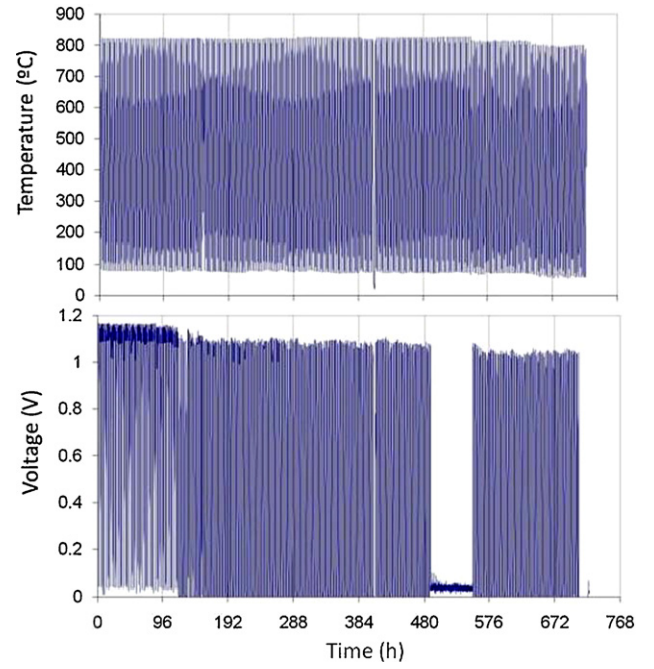

Fig. 13. Thermal cycling of a co-sintered metal-supported cell with humidified hydrogen and air. Heating and cooling occurred at 10 °C/min between 80 and 800 °C. Over 250 cycles are shown. Reproduced with permission from Ref. [10].

4. Cathode issues

Metal-supported cells fabricated by plasma spray of the electrolyte have typically utilized LSM or LSCF cathodes, also deposited by plasma spray. Although preparing cathodes with sufficient porosity was originally seen as a significant challenge [4], improved cathodes displaying adequate performance have been developed [38].

Cathode selection for cells fabricated by sintering processes is more complicated. To avoid oxidation of the metal support, sintering fabrication steps are typically conducted in reducing atmosphere. Metal-supported cells are amenable to braze-sealing [56], which also requires processing in inert or vacuum atmosphere. Standard cathode catalysts decompose in such atmospheres [1], so cathodes are generally applied to metal-supported cells after all non-oxidizing-atmosphere processing steps are complete. Cathodes are typically processed in air, but to avoid oxidation of the metal support, the maximum sintering temperature should be below about 900 °C. This severely limits the choice of cathode, as conventional compositions such as LSM and LSCF require sintering in air at the 1000–1200 °C range to achieve high performance. LSCF can be sintered well enough to bond to the electrolyte below 1000 °C, but it was reported that the poor cathode performance accounted for half of the total cell resistance for a metal-supported cell with this cathode [26]. Various cathode compositions in the (La,Sr)(Cr,Mn)$O_{3-\delta}$ family were studied to determine if they could be sintered in nitrogen at 1100 °C, a condition that would avoid oxidation of the metal support [57]. Suitable sintering was achieved, but no composition provided sufficient performance at 700–800 °C. SDC-$Sm_{0.5}Sr_{0.5}CoO_3$ (SSC) composite cathodes have been applied to metal-supported CGO-based cells because of their good low-temperature performance after firing at a relatively low temperature of 800 °C [26,30–35]. SSC has a very high thermal expansion coefficient, however, and even the SDC-SSC composite was reported to display a CTE of 18.4 ppm K^{-1}. This leads to significant cracking in the cathode during thermal cycling [33]. LSCF and SSC also contain metal oxides that tend to react easily with Cr [51], making them especially susceptible to Cr vapor coming from upstream balance-of-plant components or from defects in stainless steel interconnect coatings within the stack. LNF is highly tolerant to the presence of Cr [58–60], and good performance has been achieved with sintering temperatures as low as 800 °C [61]. These features recommend the application of LNF to metal-supported SOFCs.

Recognizing the processing limitations noted above, in particular the decomposition of LSM and other cathode catalysts in reducing or vacuum atmosphere, LBNL has developed a unique approach to cathode fabrication based on catalyst infiltration. First, a porous YSZ anode structure (with no catalyst present) is co-sintered with the metal support, electrolyte layer, and possibly other cell layers in reducing atmosphere at high temperature. Second, after further cell processing, including braze-sealing if used, the catalyst is infiltrated by the precursor method [62]. Molten salts of the metals that comprise the catalyst are flooded into the pores of the anode layer at low temperature, around 100 °C. The salts decompose to the intended oxide catalyst compositions around 400–600 °C. Processing in this manner avoids the presence of catalyst during high-temperature processing steps, so decomposition in non-oxidizing atmosphere and deleterious reactions with the electrolyte are avoided. Appropriate salts of many metals are easily available, so a wide variety of catalyst compositions can be prepared by this route, including those that would be unstable were they subjected to high-temperature processing.

Fig. 14 shows an image of a cathode prepared by infiltrating LSM into a porous YSZ backbone. The LSM forms a continuous blanket of nano-scale catalyst particles on the walls of the porous YSZ structure, providing for high triple phase boundary and good electronic percolation through the LSM phase. Because the catalyst particles are small, thermal expansion mismatch between the catalyst and YSZ backbone can be tolerated. Furthermore, the catalyst is not part of the mechanical backbone of the cell, so any stress generated by thermal expansion mismatch will not affect the integrity of the electrolyte.

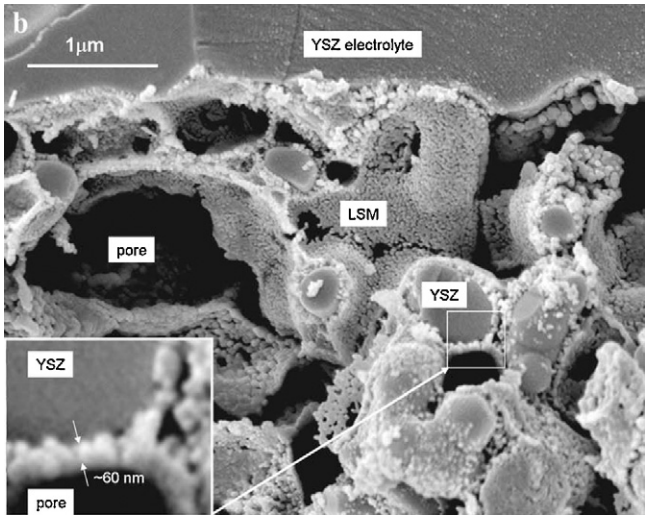

Fig. 14. SEM micrograph of fracture surface of porous YSZ electrode infiltrated with LSM catalyst. The inset shows the ~60 nm LSM catalyst layer to be well adhered to the YSZ backbone. Reproduced with permission from Ref. [62].

It should be noted that most metal-supported cells tested to date are button cells with Pt mesh or other current collection materials that do not contain Cr. Thus, realistic cathode conditions (i.e. containing Cr) have generally been avoided. One notable exception is the LBNL design, in which a porous stainless steel current collector is in direct contact with the cathode, as shown in Fig. 15. The current collector is sintered before catalyst infiltration, and it is coated by catalyst during infiltration. If the catalyst contains a rare earth element, as most do, the coating is expected to improve oxidation resistance of the current collector [43,49]. Also, the coating serves to minimize Cr evaporation from the current collector [63]. Conventional composite LSM-YSZ cathodes with direct contact to uncoated stainless steel current collectors are known to fail very quickly due to Cr poisoning, sometimes within several hours [64]. In contrast, metal-supported cells with infiltrated LSM catalyst and coating on the current collector have been operated for hundreds of hours without evidence of Cr poisoning [9,50]. Testing with infiltrated LNF is also under way.

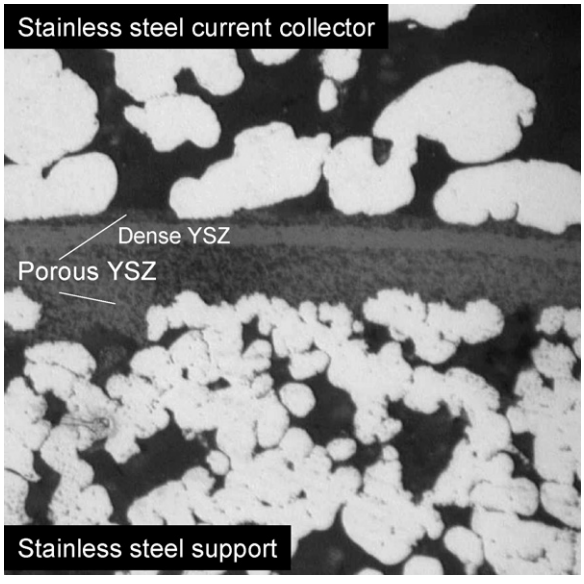

Fig. 15. Cross-section micrograph of co-sintered metal-supported cell prepared at LBNL.

5. Anode issues

As discussed above in Section 2.2.1, it is desirable to operate cells with ferritic stainless steels in the 650–700 °C range. This is a relatively low temperature for SOFC operation, and preparing anodes with high performance in this temperature range is challenging. Most MSC developers began their efforts with a cell design incorporating Ni-YSZ anode based on conventional ASC and ESC cell technology. This leads to a couple of processing issues. Firstly, any cell processing above about 900 °C should utilize non-oxidizing atmosphere, typically 4% hydrogen or high vacuum, to avoid oxidation of the metal support. Ni/NiO is reduced in such conditions, and significant coarsening can occur. This causes a decrease in triple phase boundary as well as disconnection between adjacent Ni particles and concomitant loss of electronic conduction in the anode. Coarsening is exacerbated at high temperature, and co-sintering of stainless steel and YSZ electrolyte at 1300–1400 °C leads to especially poor performance of the Ni-YSZ anode [8]. Secondly, any cell design with direct contact between a stainless steel support and Ni-containing anode suffers from interdiffusion of Ni and Fe/Cr. Regardless of electrolyte material or processing choice, this phenomenon can occur during operation of the cell [36] and is especially problematic in situations where there is direct anode/support contact during high-temperature processing steps [7,11,65]. The resulting distribution of elements is particularly well exemplified in Fig. 16. Diffusion of Ni into the ferritic stainless steel support can cause conversion to austenitic phase, resulting in significantly reduced oxidation resistance and increased CTE of the support (see Table 1). Diffusion of Fe and Cr into the Ni-containing anode can cause formation of insulating oxides such as Cr_2O_3, $NiCr_2O_4$, FeO, etc. which impair catalytic activity.

5.1. Diffusion barrier layers

Insertion of a diffusion barrier layer (DBL) has been explored extensively as a solution to Ni and Fe/Cr interdiffusion [11,36–39]. The barrier layer must prevent interdiffusion while allowing electron and gas transport, have similar CTE to the other materials, and be stable and compatible with the relevant operating and processing conditions. Compositions including: $La_{0.6}Sr_{0.2}Ca_{0.2}CrO_3$ and $La_{1-x}Sr_xMnO_3$ [36–38]; CeO_2, and $Ce_{0.8}Gd_{0.2}O_2$ [39]; and undisclosed compositions [11] were found to be effective diffusion barriers. Note that compositions similar to LSM are expected to be unstable in fuel atmosphere [1]. Cr_2O_3-based diffusion layers were also employed, but were not very effective because the Cr_2O_3 layer was reduced during high-temperature processing in reducing atmosphere [39]. A Cu-YSZ cermet DBL was found to block Ni diffusion into the support, but not completely block Fe and Cr diffusion into the anode [66].

5.2. Alternative anode designs

While use of a barrier layer is an effective means of blocking interdiffusion, it can present an extra ohmic impedance, and will not prevent Ni coarsening during high-temperature processing. Therefore, it has not been found to be an effective solution for preparing an anode that will achieve high performance at 700 °C or below. A number of alternative cell designs have been proposed to alleviate these issues. Waldbillig and Kesler [40] prepared metal-supported cells using conventional plasma spray deposition, but with the cathode applied first, followed by electrolyte and Ni-based anode. This design eliminates Ni and Fe/Cr interdiffusion during processing and introduces a number of other advantages. A DBL would likely still be required between the anode and stainless steel interconnect in a stacked configuration, however. Also, the direct intimate contact between cathode and metal support may require

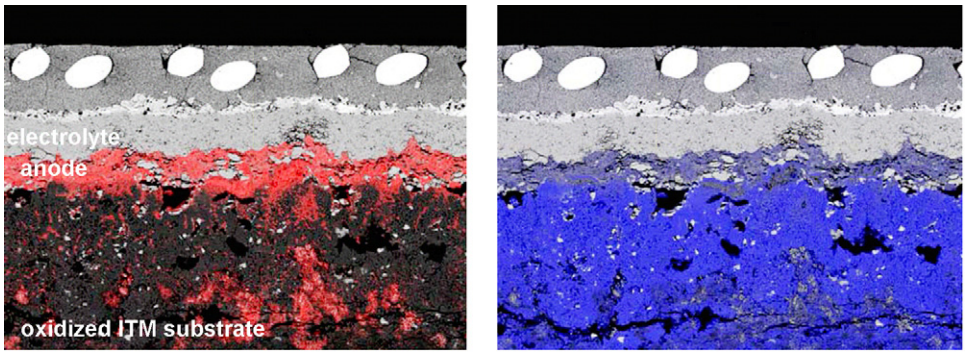

Fig. 16. EDAX/SEM composite image of cross-section of metal-supported cell produced by plasma spray processing with no diffusion barrier layer present. Images taken after 1500 h operation at 800 °C. Left image shows Ni distribution as red overlay, right image shows Cr distribution as blue overlay. Reproduced with permission from Ref. [36].

alternative cathode materials that are tolerant to the presence of Cr. Nonetheless, promising power density of >100 mW cm^{-2} was achieved for the first trials of this design.

Copper is known to be an effective SOFC anode conductor, and when used in conjunction with ceria can provide an alternative to conventional Ni-cermet electrodes. Cu (m.p. 1083 °C) melts at typical SOFC processing temperatures, normally eliminating it from consideration. It has been shown, however, that molten Cu tends to wet YSZ in typical co-sintering conditions (1300 °C, hydrogen-containing atmosphere), leading to a highly electronically conductive cermet with fine metal features [66]. Thus, Cu-YSZ may form the basis for an anode suitable for cofiring between stainless steel support and YSZ electrolyte. Initial anode performance was encouraging, although more development is needed.

5.3. Infiltrated anode design

The approach taken by LBNL, and more recently by Risoe, to address the issues of Ni interdiffusion and coarsening is to prepare the anode using the infiltration techniques developed for cathode catalysts, discussed above in Section 4 [8,9,27,50]. First, a porous YSZ anode structure (with no catalyst present) is co-sintered with the metal support, electrolyte layer, and possibly other cell layers in reducing atmosphere at high temperature. Second, after further cell processing, the catalyst is infiltrated by the precursor method, resulting in structures similar to those described in Section 4 and Fig. 14. Thus, the anode catalyst is never exposed to high-temperature reducing sintering conditions, solving the issues of interdiffusion and catalyst coarsening during cell fabrication. The anode catalyst also coats the metal support, so inclusion of rare earth salts in the catalyst precursor is expected to enhance oxidation resistance of the metal support [43,49]. As discussed for infiltrated cathode structures, above in Section 4, the catalyst is not part of the mechanical structure of the cell, but rather forms a thin coating on the YSZ and stainless steel backbone similar to the situation shown in Fig. 14. Therefore, expansion and contraction due to thermal or redox cycling does not cause stress in the electrolyte layer, and catalyst compositions with significant CTE mismatch or volume change upon redox cycling can be tolerated. Favorable redox and thermal cycling tolerance of cells with infiltrated anode design were reported in Ref. [9]. This advantage provides very flexible choice in catalyst composition.

Early work with infiltration of anode catalyst into metal-supported SOFCs focused on Ni-based anode compositions [8,9]. The well-connected network of fine Ni catalyst enabled initial power densities of almost 1 W cm^{-2} at only 650 °C. Ni does not wet YSZ well, however, and Ni coarsening during operation caused dramatic degradation in performance [9]. Moderate improvements in wetting behavior for infiltrated Ni were accomplished by precoarsening at a temperature above the operating temperature [9], and co-infiltration of TiO_2 [67]. The most promising approach to date is replacement of most or all of the Ni with an anode catalyst, such as doped ceria, that is stable in contact with YSZ in SOFC fuel conditions. Fig. 17 compares cells prepared at LBNL with infiltrated Ni and infiltrated SDC as anode catalysts; the ceria composition is dramatically more stable. Although ceria offers improved stability, its electronic conductivity is much less than that of Ni. In the case of YSZ anode backbone, all the electronic current passing from the metal support to the active electrode area is carried by the ceria catalyst coating. In such a design, cell performance may be limited by the ceria electronic conductivity. This situation can be improved by addition of a conductive component to the anode backbone, such as copper (discussed above in this section), or stainless steel particles. Risoe has demonstrated the latter choice, [27] and promising durability of the cell is shown in Fig. 12. The metal particles used in the YSZ-steel cermet anode layer were quite small, however, so long-term oxidation resistance is not expected.

In summary, infiltration of the anode catalyst alleviates cell processing issues, and results in a high-performance structure. Improvements in catalyst composition and current collection schemes are needed, and this is a fruitful area for further research.

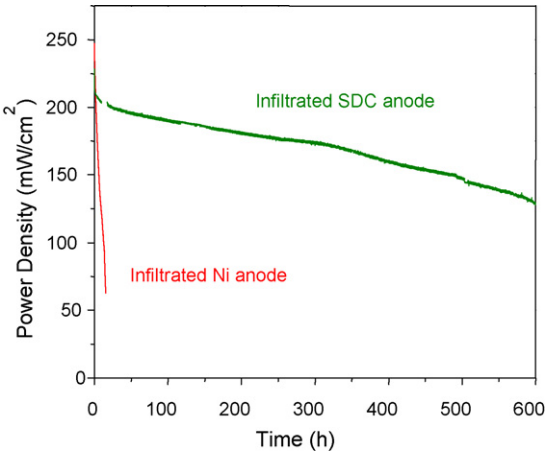

Fig. 17. Comparison of stability for co-sintered metal-supported cells with YSZ electrolyte and porous YSZ electrodes. Both cells have infiltrated LSM cathode catalyst and infiltrated Ni or SDC anode catalyst. Operation was at 700 °C with humidified hydrogen and oxygen. Data taken from Ref. [50].

6. Seals

One of the expected advantages of metal-supported SOFCs is novel sealing strategies to overcome sealing difficulties experienced with conventional all-ceramic cells. For instance, some deformation of the metal-supported cells can be tolerated, so compression seals may be effective even if the cell is not perfectly flat. Metals can be easily brazed, welded, crimped, compressed, etc. enabling new routes for sealing. Most metal-supported cells tested to date are small button cells, and conventional lab-scale sealing methods such as ceramic adhesive paste [30], ceramic felt [33] or glass seal [27] have been used for cell demonstration purposes.

A few groups have developed sealing strategies that take advantage of the unique strengths of metal-supported cells. Further work in this area is expected to produce strong, low-cost seal designs. Ceres Power reports a cell design in which the support has a dense metal perimeter [5]. Presumably, the cell active layers overlay this perimeter, providing an electrolyte to metal seal. The metal cell perimeter is then sealed to stack components using conventional metal-to-metal sealing, such as compression gaskets or laser welding. The resulting gas-tight seals survived repeated thermal cycling.

LBNL utilizes brazed seals that seal against the electrolyte, metal support, and interconnect/manifold. Active braze alloy (containing Ti) is used to promote wetting of the braze on the electrolyte surface, and Al_2TiO_5 can be added to improve the CTE match to other cell components [56]. Extremely rapid thermal cycling ($\sim$500 °C min^{-1}) was demonstrated for braze-sealed metal-supported cells with no loss of sealing. JPower extended the use of brazed seals to successfully build a short segment-in-series tubular metal-supported cell stack, achieving >1 V per cell [12].

7. R&D opportunities

Metal-supported SOFCs produced by a variety of methods are receiving increased attention from academic researchers and industrial developers. Promising demonstrations of thermal cycling, redox cycling, and adequate power density occurred, and lifetime is steadily increasing. As described in this paper, a deep fundamental understanding of the properties–structure–processing interrelationship for the various materials and cell designs has been developed. Metal-supported cells are poised for success, but significant research and development is still needed. Some of the materials and performance issues to be addressed are listed below.

Cathode:

- Long-term demonstration of Cr-tolerant cathode materials in realistic cathode conditions.
- Further development of cathode processing routes that are compatible with metal support.

Anode:

- Further development of anode compositions and structures that provide high power density at low temperature, with low-degradation rate.
- Demonstration of internal reforming and tolerance to fuel impurities.

Seals:

- Low-cost, highly manufacturable, rugged seals that take advantage of metal-to-metal joining technologies; sealing to the electrolyte is a particular challenge.

Support alloys:

- Assessment of high-temperature mechanical properties, including creep rate, burst strength, and degree of deformation accepted before electrolyte cracks or delaminates from support.
- Improvement in oxidation rate by alloying, coating, etc.
- Determination of chromia scale electronic conductivity at relevant temperatures and oxygen, hydrogen, and carbon partial pressures.

In addition to these cell materials and processing issues, significant benefit is expected from modeling metal-supported cells and stacks. Cell-level electrochemistry models can help optimize cell layer thickness, porosity, composition, etc and predict response to various fuels and control strategies. In particular, the high thermal and electronic conductivities of the support will ameliorate thermal gradients and non-uniform current distribution. It can be expected that there are advantageous stack and system designs, control strategies, and operational protocols that are only possible with metal-supported cells. Such possibilities should be explored to identify new ways that metal-supported cell technology can enable commercialization of SOFCs. For instance, the mechanical strength of the metal support may enable large differences between air-side and fuel-side pressure. This would allow optimization of the air and fuel pressure independently, potentially minimizing parasitic losses. Additionally, the ability to rapidly thermal cycle may enable a control strategy wherein the cell temperature is varied quickly to meet transient load requirements. Thus, cell voltage or current could be fixed while still providing temporary peak power at a higher temperature. Although temperature transients may temporarily reduce electrical efficiency, some waste heat recovery would be expected either within the BOP or as useful heat in a CHP application.

8. Conclusions

Metal-supported cells offer significant benefits over conventional all-ceramic solid oxide fuel cells, including low materials cost, excellent abuse tolerance, and the possibility of improved sealing and stacking schemes. Significant understanding of the materials and processing issues arising from co-processing of metal and ceramic fuel cell components has been developed. At this point, the dominant metal-supported fuel cell design consists of porous ferritic steel support and CGO or YSZ electrolyte. Promising demonstrations of redox cycling, thermal cycling, and low-degradation operation suggest that metal-supported cells are poised to overcome the barriers to commercialization of conventional SOFC technology.

Acknowledgements

This work was supported in part by the U.S. Department of Energy under Contract No. DE-AC02-05CH11231. The author thanks Grace Lau, Tal Sholklapper, Steve Visco, and Lutgard DeJonghe for helpful discussion. Special thanks go to Craig Jacobson for providing training and sharing his deep insight during my years as a newcomer to this field.

References

[1] N. Minh, T. Takahashi, Science and Technology of Ceramic Fuel Cells, Elsevier, The Netherlands, 1995.
[2] K.R. Williams, J.G. Smith, Fuel Cell with Solid State Electrolytes, US3,464,861 (1969).
[3] A. Momma, Y. Kaga, T. Okuo, K. Fujii, K. Hohjyo, M. Kanazawa, Bull. Electrotechn. Lab. 63 (1999) 103–113.

[4] G. Schiller, R.H. Henne, M. Lang, R. Ruckdäschel, S. Schaper, Fuel Cells Bull. 3 (21) (2000) 7–12.
[5] P. Bance, N.P. Brandon, B. Girvan, P. Holbeche, S. O'Dea, B.C.H. Steele, J. Power Sources 131 (2004) 86–90.
[6] N.P. Brandon, A. Blake, D. Corcoran, D. Cumming, A. Duckett, K. El-Koury, D. Haigh, C. Kidd, R. Leah, G. Lewis, C. Matthews, N. Maynard, N. Oishi, T. McColm, R. Trezona, A. Selcuk, M. Schmidt, L. Verdugo, J. Fuel Cell Sci. Technol. 1 (2004) 61–66.
[7] I. Villarreal, C. Jacobson, A. Leming, Y. Matus, S. Visco, L. DeJonghe, Electrochem. Solid State Lett. 6 (9) (2003) A178–A179;
S. Visco, et al., International Symposium on Fuel Cells for Vehicles, Nagoya, Japan, 2000;
Y.B. Matus, L.C. DeJonghe, C.P. Jacobson, S.J. Visco, Solid State Ionics 176 (2005) 443–449.
[8] M.C. Tucker, G.Y. Lau, C.P. Jacobson, L.C. DeJonghe, S.J. Visco, J. Power Sources 171 (2007) 477–482.
[9] M.C. Tucker, G.Y. Lau, C.P. Jacobson, L.C. DeJonghe, S.J. Visco, J. Power Sources 175 (2008) 447–451.
[10] L.M. Rodriguez-Martinez, L. Otaegi, M.A. Alvarez, M. Rivas, N. Gomez, A. Zabala, N. Arizmendiarrieta, I. Antepara, M. Olave, A. Urriolabeitia, I. Villarreal, A. Laresgoiti, ECS Trans. 25 (2) (2009) 745–752.
[11] I. Villarreal, M. Rivas, L.M. Rodriguez-Martinez, L. Otaegi, A. Zabala, N. Gomez, M.A. Alvarez, I. Antepara, N. Arizmendiarrieta, J. Manzanedo, M. Olave, A. Urriolabeitia, N. Burgos, F. Castro, A. Laresgoiti, ECS Trans. 25 (2) (2009) 689–694.
[12] S. Sakuno, S. Takahashi, H. Sasatsu, ECS Trans. 25 (2) (2009) 731–737.
[13] A. Mineshige, K. Fukushima, S. Okada, T. Kikuchi, M. Kobune, T. Yazawa, K. Kikuchi, M. Inaba, Z. Ogumi, Electrochem. Solid-State Lett. 9 (2006) A427–A429.
[14] C. Hwang, C.-H. Tsai, C.-H. Lo, C.-H. Sun, J. Power Sources 180 (2008) 132–142.
[15] H.J. Cho, G.M. Choi, Solid State Ionics 180 (2009) 792–795.
[16] T. Ishihara, J. Yan, M. Enoki, S. Okada, H. Matsumoto, J. Fuel Cell Sci. Technol. 5 (2008) 031205-1–031205-3.
[17] Y.W. Ju, H. Eto, T. Inagaki, T. Ishihara, ECS Trans. 25 (2) (2009) 719–726.
[18] J. Yan, M. Enoki, H. Matsumoto, T. Ishihara, Electrochem. Solid-State Lett. 10 (2007) B139–B141.
[19] T. Ishihara, J. Yan, M. Shinagawa, H. Matsumoto, Electrochim. Acta 52 (2006) 1645–1650.
[20] Y. Lee, G.M. Choi, ECS Trans. 25 (2) (2009) 727–730.
[21] H.C. Park, A.V. Virkar, J. Power Sources 186 (2009) 133–137.
[22] J.H. Zhu, S.J. Geng, Z.G. Lu, W.D. Porter, J. Electrochem. Soc. 154 (2007) B1288–B1294.
[23] P.Y. Hou, J. Stringer, Mater. Sci. Eng. A202 (1995) 1–10;
P.Y. Hou, K. Huang, W.T. Bakker, Promises and problems with metallic interconnects for reduced temperature solid oxide fuel cells, in: S.C. Singhal, et al. (Eds.), Proceedings of the 6th International Symposium on Solid Oxide Fuel Cells (SOFC-VI), Honolulu, Hawaii, October 17–22, 1999.
[24] S. Molin, M. Gazda, B. Kusz, P. Jasinski, J. Eur. Ceram. Soc. 29 (2009) 757–762.
[25] Z. Yang, Int. Mater. Rev. 53 (2008) 39–54.
[26] N. Oishi, Y. Yoo, ECS Trans. 25 (2) (2009) 739–744.
[27] P. Blennow, J. Hjelm, T. Klemensø, Å. Persson, K. Brodersen, A.K. Srivastava, H.L. Frandsen, M. Lundberg, S. Ramousse, M. Mogensen, ECS Trans. 25 (2) (2009) 701–710.
[28] R.A. Andrievskii, V.S. Pugin, I.M. Fedorchenko, B.Z. Teverovskii, Poroshkovaya Metallurgiya 1 (1965) 20–31.
[29] R.T. Leah, N.P. Brandon, P. Aguiar, J. Power Sources 145 (2005) 336–352.
[30] R. Hui, D. Yang, Z. Wang, S. Yick, C. Decès-Petit, W. Qua, A. Tuck, R. Maric, D. Ghosh, J. Power Sources 167 (2007) 336–339.
[31] Y. Xie, R. Neagu, C.-S. Hsu, X. Zhang, C. Decès-Petit, J. Electrochem. Soc. 155 (4) (2008) B407–B410.
[32] Q.-A. Huang, J. Oberste-Berghaus, D. Yang, S. Yick, Z. Wang, B. Wang, R. Hui, J. Power Sources 177 (2008) 339–347.
[33] Z. Wang, J. Oberste Berghaus, S. Yick, C. Decès-Petit, W. Qu, R. Hui, R. Maric, D. Ghosh, J. Power Sources 176 (2008) 90–95.
[34] R. Hui, J.O. Berghaus, C. Decès-Petit, W. Qu, S. Yick, J.-G. Legoux, C. Moreau, J. Power Sources 191 (2009) 371–376.
[35] Q.-A. Huang, B. Wang, W. Qu, H. Rob, J. Power Sources 191 (2009) 297–303.
[36] T. Franco, K. Schibinger, Z. Ilhan, G. Schiller, A. Venskutonis, ECS Trans. 7 (1) (2007) 771–780.
[37] T. Franco, M. Brandner, M. Rüttinger, G. Kunschert, A. Venskutonis, L.S. Sigl, ECS Trans. 25 (2) (2009) 681–688.
[38] P. Szabo, J. Arnold, T. Franco, M. Gindrat, A. Refke, A. Zagst, A. Ansar, ECS Trans. 25 (2) (2009) 175–185.
[39] M. Brandner, M. Bram, J. Froitzheim, H.P. Buchkremer, D. Stöver, Solid State Ionics 179 (2008) 1501–1504;
M. Bradner, Dissertation, Univ. Bochum (2006) http://juwel.fz-juelich.de:8080/dspace/bitstream/2128/2552/1/Juel_4238_Brandner.pdf.
[40] D. Waldbillig, O. Kesler, J. Power Sources 191 (2009) 320–329.
[41] H. Kurokawa, G.Y. Lau, C.P. Jacobson, L.C. De Jonghe, S.J. Visco, J. Mater. Processing Technol. 182 (2007) 469–476.
[42] J.W. Fergus, Mater. Sci. Eng. A 397 (2005) 271–283.
[43] N. Shaigan, W. Qu, D.G. Ivey, W. Chen, J. Power Sources 195 (2010) 1529–1542.
[44] H. Kurokawa, K. Kawamura, T. Maruyama, Solid State Ionics 168 (2004) 13–21.
[45] J. Webber, Corros. Sci. 16 (1976) 499–506.
[46] A. Holt, P. Kofstad, Solid State Ionics 69 (1994) 137–143.
[47] H. Liu, M.M. Stack, S.B. Lyon, Solid State Ionics 109 (1998) 247–257.
[48] P. Huczkowski, N. Christiansen, V. Shemet, L. Niewolak, J. Piron-Abellan, L. Singheiser, W.J. Quadakkers, Fuel Cells 6 (2006) 93–99.
[49] I. Belogolovsky, P.Y. Hou, C.P. Jacobson, S.J. Visco, J. Power Sources 182 (2008) 259–264.
[50] M.C. Tucker, T.Z. Sholklapper, G.Y. Lau, L.C. DeJonghe, S.J. Visco, ECS Trans. 25 (2) (2009) 673–680.
[51] M.C. Tucker, H. Kurokawa, C.P. Jacobson, L.C. De Jonghe, S.J. Visco, J. Power Sources 160 (2006) 130–138.
[52] C. Kleinlogel, L.J. Gauckler, Solid State Ionics 135 (2000) 567–573.
[53] G.S. Lewis, A. Atkinson, B.C.H. Steele, J. Drennan, Solid State Ionics 152–153 (2002) 567–573.
[54] J.D. Nicholas, L.C. DeJonghe, Solid State Ionics 178 (2007) 1187–1194.
[55] R. Henne, J. Thermal Spray Technol. 16 (3) (2007) 381–403.
[56] M.C. Tucker, C.P. Jacobson, L.C. De Jonghe, S.J. Visco, J. Power Sources 160 (2006) 1049–1057.
[57] S.W. Baek, J. Jeong, S. Lee, J. Bae, ECS Trans. 25 (2) (2009) 2909–2914.
[58] T. Komatsu, H. Arai, R. Chiba, K. Nozawa, M. Arakawa, K. Sato, Electrochem. Solid-State Lett. 9 (2006) A9–A12.
[59] T. Komatsu, H. Arai, R. Chiba, K. Nozawa, M. Arakawa, K. Sato, J. Electrochem. Soc. 154 (2007) B379–B382.
[60] M. Stodolny, F.P.F. van Berkel, B.A. Boukamp, ECS Trans. 25 (2) (2009) 2915–2922.
[61] H. Orui, K. Watanabe, R. Chiba, M. Arakawa, J. Electrochem. Soc. 151 (2004) A1412–A1417.
[62] T.Z. Sholklapper, C. Lu, C.P. Jacobson, S.J. Visco, L.C. De Jonghe, Electrochem. Solid-State Lett. 9 (2006) A376–A378.
[63] H. Kurokawa, C.P. Jacobson, L.C. DeJonghe, S.J. Visco, Solid State Ionics 178 (2007) 287–296.
[64] S.P. Jiang, Y.D. Zhen, S. Zhang, J. Electrochem. Soc. 153 (8) (2006) A1511–A1517.
[65] H.J. Cho, Y.M. Park, G.M. Choi, ECS Trans. 25 (2) (2009) 695–699.
[66] M.C. Tucker, C.P. Jacobson, Cu-based cermet for high-temperature fuel cell, US2007117006(A1) (2009);
M.C. Tucker, G.Y. Lau, C.P. Jacobson, S.J. Visco, L.C. De Jonghe, Cu-YSZ cermet solid oxide fuel cell anode prepared by high-temperature sintering, J. Power Sources 195 (10) (2010) 3119–3123.
[67] C.A. Singh, L. Bansal, P. Tiwari, V.V. Krishnan, ECS Trans. 25 (2) (2009) 1897–1904.
[68] Haynes, Hastelloy X Alloy, Haynes International (1997) http://www.haynesintl.com/pdf/h3009.pdf.
[69] D. Sacriste, N. Goubot, J. Dhers, M. Ducos, A. Vardelle, J. Thermal Spray Technol. 10 (2001) 352–358.
[70] J. Matejicek, S. Sampath, P.C. Brand, H.J. Prask, Acta Mater. 47 (1999) 607–617.